JTTEE5 19:275–285
DOI: 10.1007/s11666-009-9415-1
1059-9630/$19.00 © ASM International

Dry Sliding Behavior of Sub-Micrometer-Sized Suspension Plasma Sprayed Ceramic Oxide Coatings

Geoffrey Darut, Fadhel Ben-Ettouil, Alain Denoirjean, Ghislain Montavon, Hélène Ageorges, and Pierre Fauchais

(Submitted April 23, 2009; in revised form August 28, 2009)

Almost half of the energy produced by an automotive engine is dissipated by friction in the cylinders, the clutch, etc. In the context of reduction of the emissions of greenhouse gases (GHGs) to mitigate climate global warming (CGW), reduction of energy losses due to friction is a critical issue. Surface treatments appear in such a context, as never than before, to be able to provide pertinent solutions to improve sliding behavior of mechanical parts. Numerous studies have clearly shown that decreasing the scale of coating structure below the micrometer scale was leading to an improvement of its tribological behavior in terms of friction coefficient and wear rate thanks to improved mechanical properties, the toughness in particular. Suspension Plasma Spraying (SPS) appears as a thermal spray process to be able to manufacture thick (i.e., a few tens of micrometers) coatings exhibiting a sub-micrometer-sized or even a nanometer-sized architecture, while keeping the versatility and flexibility of the thermal spray routes: i.e., the ability to process a wide range of material natures onto a wide range of substrate materials of various geometries. This article aims at studying the tribological behavior of several ceramic oxide composite coatings under dry conditions. The structural scale and the effect of composition are considered in particular.

Keywords alumina, friction coefficients, silicon carbide, sub-micrometer-sized coating, suspension plasma spraying, wear rate, zirconia

1. Introduction

Nanomaterials are nowadays an incontrovertible subject of research. The benefit provided by nanomaterials does not need to be proven anymore in numerous fields. With their structural size being decreased, properties of materials, for example, the mechanical strength, the thermal diffusivity, the electrical resistivity, etc. are improved (Ref 1). Numerous processes can be implemented to manufacture nanostructured coatings (Ref 2). Regarding tribological behavior, the incorporation of nanoparticles into coatings (Ref 3) or the manufacturing of bulk structures embedding nanocrystalline materials (Ref 4) leads to improvement of their wear resistances. Explanation resides in the fact that reducing the structural scale of materials increases the density of atoms along grain boundaries, increasing, in turn, strength and toughness (Ref 5).

Another way of improving the tribological behavior of coatings is to manufacture composite coatings incorporating reinforcement materials inside a matrix such as ZrO_2 in Al_2O_3 matrix (Al_2O_3-ZrO_2), TiO_2 in Al_2O_3 (Al_2O_3-TiO_2), SiC in Ni (Ni-SiC), etc. Indeed, coating fracture toughness is increased with the addition of zirconia or titania in alumina coating (Ref 6, 7) or wear resistance is improved by incorporation of SiC particles in Ni matrix (Ref 8).

Thermal spraying is a process permitting to manufacture coatings with sub-micrometer scale structure, or even nanometer scale in some cases. Two routes can be implemented:

- The first one considers a gas as carrier of micrometer-sized particles made of agglomeration of nano-sized particles. After selecting the due operating parameters, powder particles are semi-molten in the thermal flow and the resulting coatings exhibit a two-scale structure: a micrometer scale corresponding to molten parts of particles (outer shell) and a sub-micrometer scale corresponding to unmolten (core) ones (Ref 9). This ultimately leads to coatings with ''bimodal'' characteristics (i.e., a combination of ''micro'' and ''nano'' properties).

This article is an invited paper selected from presentations at the 2009 International Thermal Spray Conference and has been expanded from the original presentation. It is simultaneously published in *Expanding Thermal Spray Performance to New Markets and Applications: Proceedings of the 2009 International Thermal Spray Conference*, Las Vegas, Nevada, USA, May 4-7, 2009, Basil R. Marple, Margaret M. Hyland, Yuk-Chiu Lau, Chang-Jiu Li, Rogerio S. Lima, and Ghislain Montavon, Ed., ASM International, Materials Park, OH, 2009.

Geoffrey Darut, Fadhel Ben-Ettouil, Alain Denoirjean, Ghislain Montavon, Hélène Ageorges, and **Pierre Fauchais**, SPCTS-UMR CNRS 6638, Faculty of Sciences and Technologies, University of Limoges, 123 Avenue Albert Thomas, 87060 Limoges cedex, France. Contact e-mails: geoffrey.darut@unilim.fr and ghislain.montavon@unilim.fr.

- The second one considers a liquid as carrier of submicrometer or nanometer-sized particles dispersed in a liquid to form a suspension (Ref 10). Depending on the operating parameters, different architectures, from fairly dense to porous with different void network architectures can be manufactured depending on the application (Ref 11).

Suspension plasma spraying (SPS) was considered in this study. The principle is based on the mechanical injection of a continuous stream of suspension made of a liquid phase, particles and a dispersant in a plasma jet, where it encounters first fragmentation in droplets due to shear forces imparted by the plasma flow before liquid phase vaporization from droplets and melting of solid particles prior to impact on the substrate to form a coating of minimal thickness of about 10 μm.

The objective of this study is to investigate tribological (friction coefficient and wear rate) behaviors of several ceramic composite coatings of various compositions, scales, and structures. Coating materials used were Al_2O_3, ZrO_2, and SiC.

2. Experimental Protocols

2.1 Process and Related Operating Parameters

The coatings were manufactured with a d.c. stick-type cathode plasma torch with an internal diameter of 5 mm developed in-house. Two different combinations of binary plasma forming gases were used: Ar-He and Ar-H_2 permitting to operate the plasma torch under takeover or restrike mode, respectively. Spray parameters are presented in Table 1. Injection was performed through a calibrated diaphragm with average diameter of 150 μm. Adjustment of the pressure in pressurized containers into which suspensions were stored permitted to control the suspension momentum density on penetration into the plasma flow.

Two different plasma forming gases have been selected to evidence the influence of plasma fluctuations (Fig. 1) on coating structures and on tribological performances. An Ar-He plasma gas mixture permits to operate the plasma torch under the takeover operating mode corresponding to low fluctuations: $\Delta V/V < 0.3$ (where ΔV is the maximal amplitude of arc voltage and V the average arc voltage). Addition of a diatomic gas such as H_2 (Ar-H_2 mixture) to the plasma gas mixture results in superior fluctuations with a $\Delta V/V$ ratio of about 1; the plasma torch is said to be operated under the restrike mode. Of course, large fluctuations lead to significant variations in thermal and kinetic histories of particles upon impact. In parallel, two operating parameters corresponding to two significantly different enthalpy values were selected to evidence the criticality of plasma energy required for particle treatment after liquid phase vaporization.

Substrates were made of low carbon steel coupons of 50 mm in diameter and 5 mm in thickness for tribological tests, and 25 mm in diameter and 20 mm in thickness for microstructural quantifications (both have the same volume: i.e., the same calorific capacity of about 38 J K^{-1}). Prior to spraying, surfaces to be covered were degreased by immersion in ethanol vapors and grit-blasted with white corundum (α-Al_2O_3) particles of 250 μm in mean diameter to achieve an average roughness (Ra) of about 2.8 ± 0.3 μm (average value and associated standard deviation resulting from 12 randomly located measurements).

2.2 Feedstock and Suspensions

Two types of alumina powders were investigated. The first is the α-Al_2O_3 P172SB supplied by Alcan (Saint-Jean de Maurienne, France) with an average size (d_{50}) of

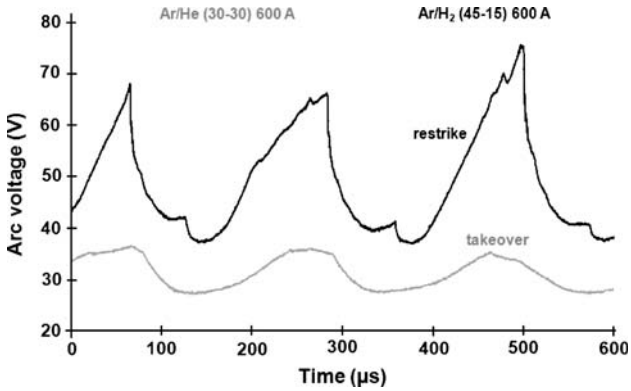

Fig. 1 Recorded voltage fluctuations for two different plasma forming gas mixtures

Table 1 Plasma spray process parameters

Designation	A	B	C
Primary plasma gas flow rate, L min^{-1}	30 (Ar)	54 (Ar)	45 (Ar)
Secondary plasma gas flow rate, L min^{-1}	30 (He)	6 (H_2)	15 (H_2)
Arc current intensity, A	600	450	500
Net power in plasma flow, kW	20	19	27
Mass enthalpy, MJ kg^{-1}	11.5	8.5	12.0
Plasma torch operating mode ($\Delta V/V$)	Take over (~0.3)	Restrike (~1.0)	Restrike (~1.0)
Torch scan velocity, m s^{-1}		1	
Scanning step, mm $pass^{-1}$		10	
Spray distance, mm		30	

Table 2 Suspension characteristics

Designation	172	30	Si		Zr	
Particles	Al_2O_3	Al_2O_3	Al_2O_3	SiC	Al_2O_3	Y-PSZ
d_{50} of particle size distribution, nm	400	300	300	3000	300	400
Liquid phase	Et-OH (99.5%)					
Powder reference	P172SB	AKP30	AKP30	Mecachrome	AKP30	001-H
wt.% of powder/suspension wt.	10					
wt.% of material/powder wt.	100		75	25	60	40
wt.% of dispersant/powder wt.	1.0		1.5		1.5	

400 nm. The second one is the α-Al_2O_3 AKP30 supplied by Sumitomo Chemical Corp. (Tokyo, Japan) with an average size (d_{50}) of 300 nm. Silicon carbide powder was contributed by Mecachrome (Tours, France) and had an average size (d_{50}) of 3 μm. Yttria-partially stabilized zirconia (Y-PSZ), with an average size (d_{50}) of 400 nm, was supplied by Unitec Ceramics (Stafford, England) as FYT13.0-001H.

Ethanol-based suspensions were prepared with ultrasonic and magnetic stirring. Composition and mass percentages are detailed in Table 2.

2.3 Characterization Techniques

Powders and coatings were observed by scanning electron microscopy in secondary electron or backscattered modes (SE-SEM and BSE-SEM, respectively) and field emission scanning electron microscopy (FESEM). Cross sections and wear tracks were invested in the same way. X-ray diffraction (XRD) was performed to quantify powder and coating phase compositions. A Siemens D5000 diffractometer equipped with a Cu anti-cathode (λ = 1.54 Å) was used with the following data acquisition parameters: 20-80° 2θ angle range, and 0.04° scanning step. Estimation of phase percentages has been determined by comparing pick heights. This semi-quantitative method permits only to determine orders of magnitude.

Coating void contents were not determined due to the lack of adequate protocols. Indeed, void content quantification performed using stereological protocols coupled with image analysis carried out on BSE-SEM randomly captured pictures along the structure to be analyzed was non-conclusive due to difficulties in polishing sample cross sections without inducing artifacts (pull-outs, scratches, etc.) and due to the too limited resolution (i.e., in the order of 200 nm) of the images, of the same order as the coating structure size. Archimedean's porosimetry was non-conclusive as well due to the too small weight of samples that were manufactured, leading to relative errors much higher than measured values. Finally, Ultra-small-angle x-ray scattering (USAXS) measurements were non-conclusive due to the too high noise/signal ratio induced by the strong absorption of radiation by alumina matrix.

Tribological tests were performed using a ball-on-disc tribometer (CSM Intruments, Lausanne, Switzerland). Operating parameters consisted of a normal load of 2 N, a linear speed of 0.1 m s^{-1}, a sintered α-Al_2O_3 counter material ball of 6 mm in diameter, and a sliding distance of 1500 m (corresponding to 23873 cycles). Tests were performed in dry mode, and wear debris were removed constantly from wear track by compressed air. Wear rate was calculated in accordance with:

$$k = \frac{V}{L \times l} \quad \text{(Eq 1)}$$

where k is the wear rate (μm^3 N^{-1} m^{-1}), V the volume lost by wear (μm^3), L the load applied (N) and l the sliding distance (m). The worn volume was measured from the wear track profile. Ten randomly located measurements were performed on each wear track and values were averaged after adjustment of 20% (i.e., the highest and the lowest values were discarded). Roughness and track profiles were measured using a Taylor Hobson (Leicester, England) surface profiler equipped with a diamond tip of 5-μm radius.

3. Results and Discussions

The first part of this study deals with the study of alumina coatings. The second one exposes reinforcement effects of alumina matrix by secondary phase particles.

3.1 Alumina Coatings

3.1.1 Feedstock. Figure 2 displays the morphology of the two different alumina powders used in this study. P172SB powder (Fig. 2a) presents a broader particle size than AKP30 one (Fig. 2b) which is more homogenous in size distribution and smaller.

3.1.2 Coating Architecture and Phase Content. Figure 3 displays cross sections of coatings resulting from the spraying of two different suspensions (172 and 30 in Table 2) using operating conditions depicted in Table 1. Cross sections show no major differences between both coating structures where voids are distinguished, but no apparent cracks at the picture resolution (about 0.2 μm). SEM is not suitable to provide pertinent information related to the SPS coating structures due to too limited resolution and the presence of numerous artifacts resulting from sample polishing (one can assume that most of the detectable ''voids'' correspond to pull-outs and scratches). Only the coating thicknesses can be reported from those views and the average deposited thickness per pass calculated, as displayed in Table 3. For alumina coatings manufactured using AKP30 powder, the highest value, 0.78 μm/pass, is obtained with operating conditions A: Ar-He (30-30) 600 A. This set of operating conditions

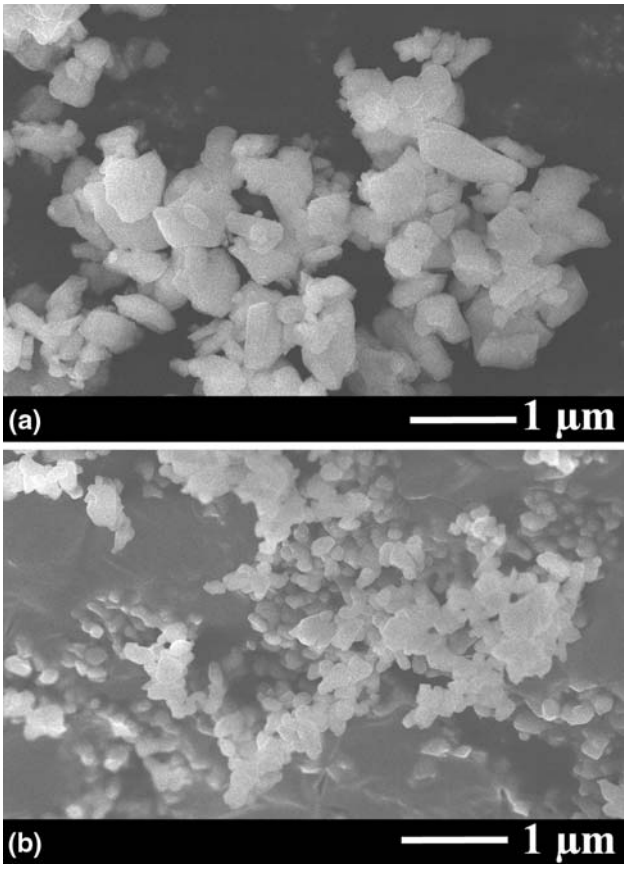

Fig. 2 SE-SEM views of morphologies of alumina powders: (a) P172SB and (b) AKP30

permits to operate the plasma torch under the takeover mode characterized by low amplitude voltage fluctuations. More particles are, hence, well treated (i.e., molten) by the plasma flow leading to a thicker deposited thickness per pass (i.e., a higher intrinsic deposition rate). It appears also that when using an Ar-H_2 (54-6) plasma gas mixture, the average thickness deposited per pass is higher than that when using an Ar-H_2 (45-15) mixture. This is very likely due to the smaller fraction of hydrogen. As a result, voltage fluctuations are lower in amplitude. and more particles forming the coating are well treated. These values confirm the inconvenience of high amplitude plasma fluctuations for homogeneous particle treatments.

Figure 4 displays the typical fracture facies of a SPS alumina coating. It is possible to easily distinguish typical features composing the coating structure: (i) flattened particles forming lamellae corresponding to well-treated (i.e., fully molten) particles, (ii) irregular (blocky) particles corresponding to untreated (i.e., unmolten) particles since they keep the initial morphology of the feedstock (fused and crushed manufacturing route), and (iii) near-spherical (''granular'') particles that predominate in the coating structure leading to the typical granular facieses. The presence of these near-spherical particles could be due to: (i) the resolidification of partially or fully molten particles prior their impact on the substrate, (ii) the poor flattening ratio of fully molten particles impacting the substrate with a too low momentum, and/or (iii) the surface tension effect due to the small size of impinging particles. Indeed, and due to the short spray distances (30 mm), the heat flux imparted by the plasma to the substrate is very high (higher than 20 MW m^{-2}) leading to a high surface temperature during spraying, well above 1000 °C (Fig. 5). This high surface temperature could significantly delay the solidification of impinging molten particles. As they would consequently remain longer on the substrate surface in a molten state and due to their small volume, surface tension would act and could involve the partial or complete recoil of the particles.

Figure 6 depicts several fracture facies of SPS alumina coatings manufactured with different suspensions and operating parameter sets. At first, it appears that particles resulting from processing of suspension 30 are better processed than the ones resulting from suspension 172. With this latter suspension, numerous small spherical and irregular particles are embedded in the coating whereas with the suspension 30, more particles are better spread. Since the AKP30 feedstock exhibits a narrower particle size distribution, particles are treated more homogenously in the plasma flow despite plasma fluctuations. This demonstrates the criticality of the feedstock size distribution on the coating structure: the narrower the size distribution, the more the homogeneous the coating structure, for a given set of operating parameters.

The effect of the plasma gas mixture on the coating structure can also be identified by considering coating fracture facies depicted in Fig. 6(b) and (d). A plasma gas mixture (Ar-H_2) inducing a restrike plasma torch operating mode leads to more untreated and resolidified particles (Fig. 6d) in comparison with a plasma gas mixture (Ar-He) inducing a takeover plasma torch operating mode (Fig. 6b), for the same enthalpy (between sets 30A and 30C, the enthalpy relative difference is about 4%, both values can be considered as identical in a first approximation). Under the restrike operating mode, particles do not spread as well as under the takeover mode, and more small spherical particles are embedded in the coating structure. In fact, plasma flow fluctuations lead to poorly treated particles.

The effect of the plasma flow mass enthalpy can be evidenced by comparing coating fracture facies depicted in Fig. 6(c) and (d): considering an Ar-H_2 plasma gas mixture, the decrease in the plasma enthalpy emphasizes the poor particle treatment. A plasma mass enthalpy of about 8.5 MJ kg^{-1} appears to be below the minimal critical enthalpy required to process adequately alumina particles (Fig. 6c) whereas a mass enthalpy of about 12 MJ kg^{-1} seems to be high enough (in the considered operating conditions).

In parallel, coatings have been manufactured on a ''smooth'' substrate (Fig. 3e) (average roughness Ra of 0.07 µm, average peak-to-valley ratio Rymax of 0.72 µm) to study the influence of the structural scale on their tribological behavior by comparing results with a previously published study (Ref 13).

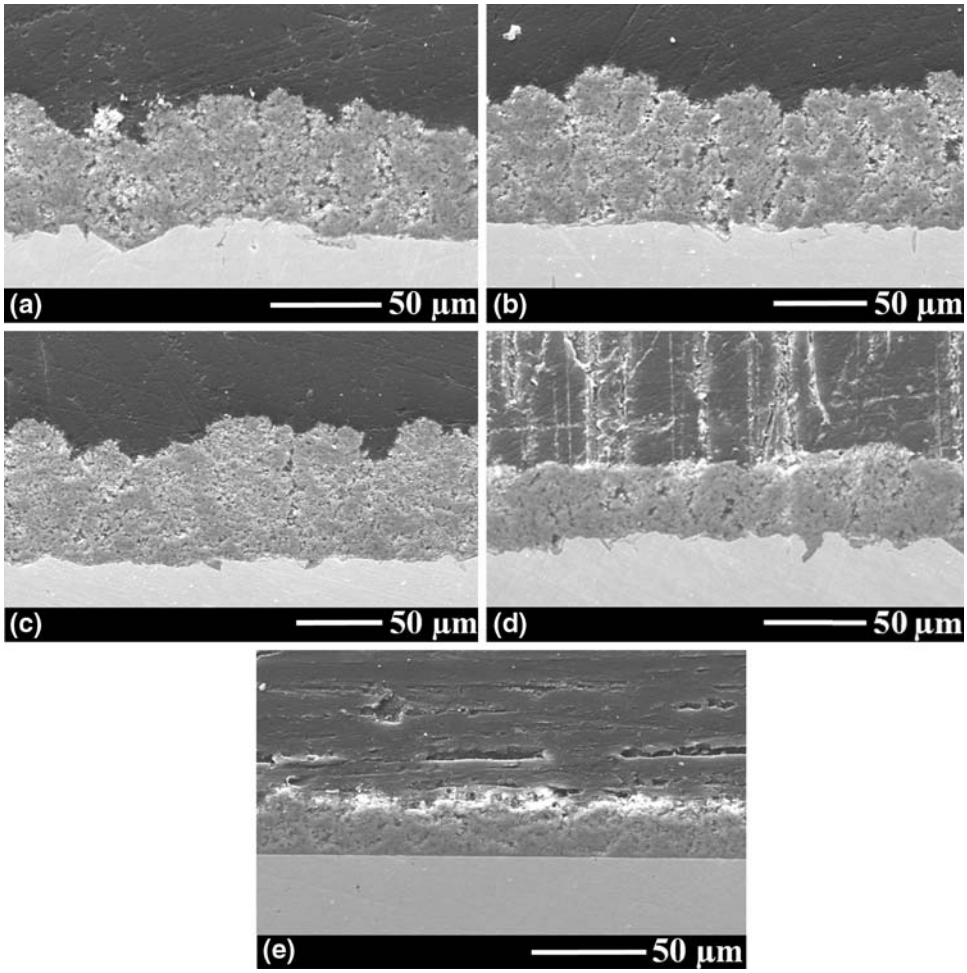

Fig. 3 SE-SEM views of cross sections of different alumina coatings manufactured with different parameters: (a) 172A, (b) 30A, (c) 30B, (d) 30C, and (e) 30As (smooth substrate)

Table 3 Average thicknesses deposited per pass and wear rates of alumina coatings (see Table 1 for designation)

Designation	172A	30A	30B	30C	30As	ZrA	SiA
Average thickness deposited per pass, µm	0.70	0.78	0.70	0.64	0.82	0.58	0.53
Wear rate, 10^3 µm^3 N^{-1} m^{-1}	100 ± 25	86 ± 17	990 ± 154	202 ± 48	57 ± 5	73 ± 16	95 ± 15

Average values and associated standard deviations from eight values resulting from ten randomly located measurements with an adjustment of 20%

Phase compositions of powders and coatings are presented in Fig. 7 and 8. The two alumina powders are made of α-Al_2O_3. For suspension plasma spraying (SPS), the predominant phase in the coatings is the α phase. Such a high content of α phase does not result, of course, from a high fraction of unmolten particles (see, for example, Fig. 6a). In such a case, moreover, coatings would not be as dense and cohesive as they are. In conventional atmospheric plasma spraying (APS) process, coatings resulting from the spraying of pure α-Al_2O_3 are mainly composed of γ phase and the remaining of α phase with a corresponding proportion depending on the operating parameters (in fact, the ratio of unmolten particles embedded in the coating) (Ref 14). In SPS, the high fraction of α-Al_2O_3 results very likely from the very short spray distance (30 mm), and, consequently from the high thermal flux imparted by the plasma flow to the substrate (in the 20 MW m^{-2} range), the transient temperature of the deposited coating when the plasma torch passes in front of a given location increases. If such a transient temperature is above 900 °C, then phase transitions occur (i.e., in situ annealing), and γ-Al_2O_3 evolves toward α-Al_2O_3 via transition alumina (δ and θ phases).

3.1.3 Friction Coefficient and Wear Rate. Before the friction tests, samples were polished with SiC paper to obtain similar surface roughnesses. Surface parameters

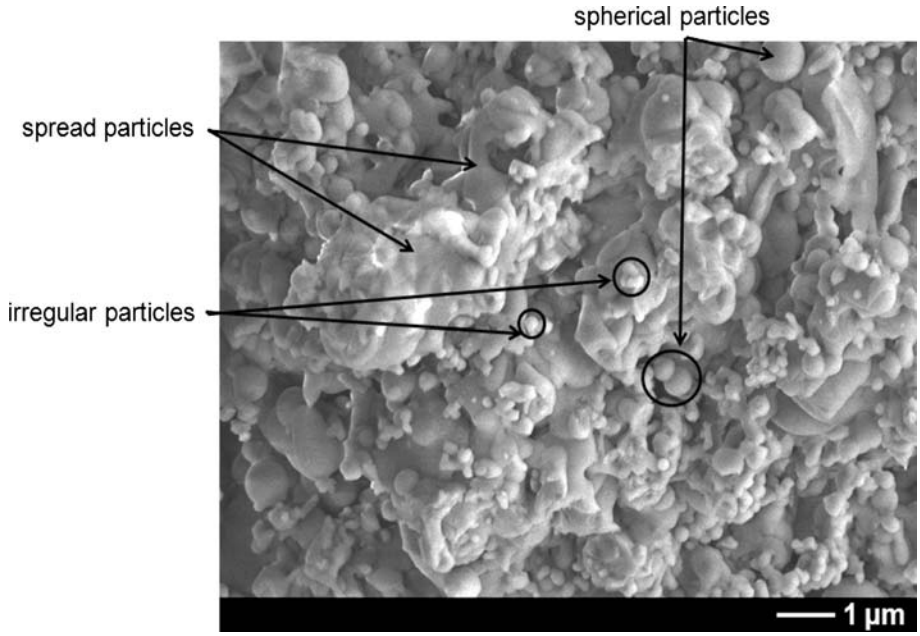

Fig. 4 Typical FESEM fracture facies of a SPS alumina coating

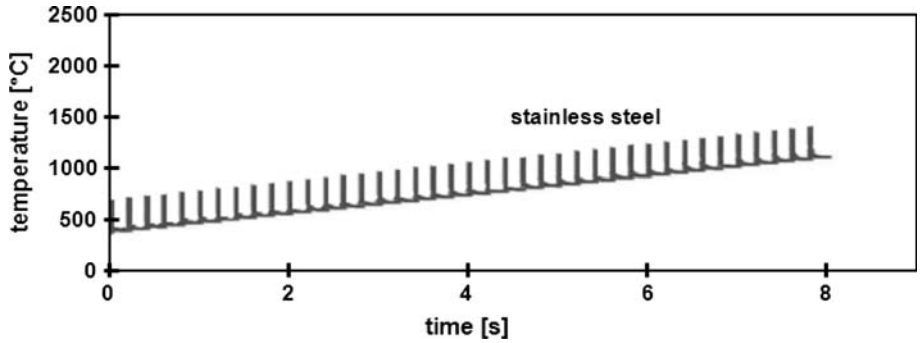

Fig. 5 Evolution of surface temperature during suspension plasma spraying of YSZ onto a stainless steel substrate (Ref 12)

after polishing are listed in Table 4. The two coatings manufactured with an Ar-H_2 mixture were delaminated during polishing, an evidence of a poor resistance to wear. Figure 9 displays the friction coefficient evolution versus sliding distance of several alumina coatings sprayed with different operating conditions.First, by comparing behaviors of coatings manufactured with the two considered alumina powders and identical operating parameters (172A and 30A), the average friction coefficient of coating 30A is slightly lower than the one of coating 172A (0.4 and 0.5, respectively). Indeed, feedstock 30 exhibits a narrower particle size distribution compared to feedstock 172. This leads to a more homogeneous thermal treatment of particles, as seen in Fig. 6, leading to a lower stacking defect density in the coating, improving its friction behavior by reducing particle exfoliation thanks to a higher coating cohesion. Indeed, the effect of particle size distribution on structure homogeneity and stacking defect density has been previously demonstrated by Delbos considering Y-PSZ feedstock (Ref 15). Also, the wear rate of the coating manufactured with P172SB powder is slightly higher than the one of the coating manufactured with AKP30 as depicted in Table 3. This corroborates the previous analysis.

Second, a coating manufactured with an Ar-He mixture (30A) presents a slightly higher friction coefficient than the one manufactured with an Ar-H_2 mixture (30C) with the same plasma mass enthalpy. However, the wear rate is more than twice lower than that of the Ar-H_2 one. Operating the plasma torch under an Ar-H_2 gas mixture leads to arc root fluctuations of higher amplitudes (restrike mode: $\Delta V/V \sim 1$ compared to the ones encountered when operating the plasma torch under an Ar-He gas mixture corresponding to a takeover mode: $\Delta V/V \sim 0.3$ (Ref 16). This leads to a less homogeneous treatment of the suspension: droplets issued from the suspension stream fragmentation exhibit a broader size distribution and more dispersed trajectories within the

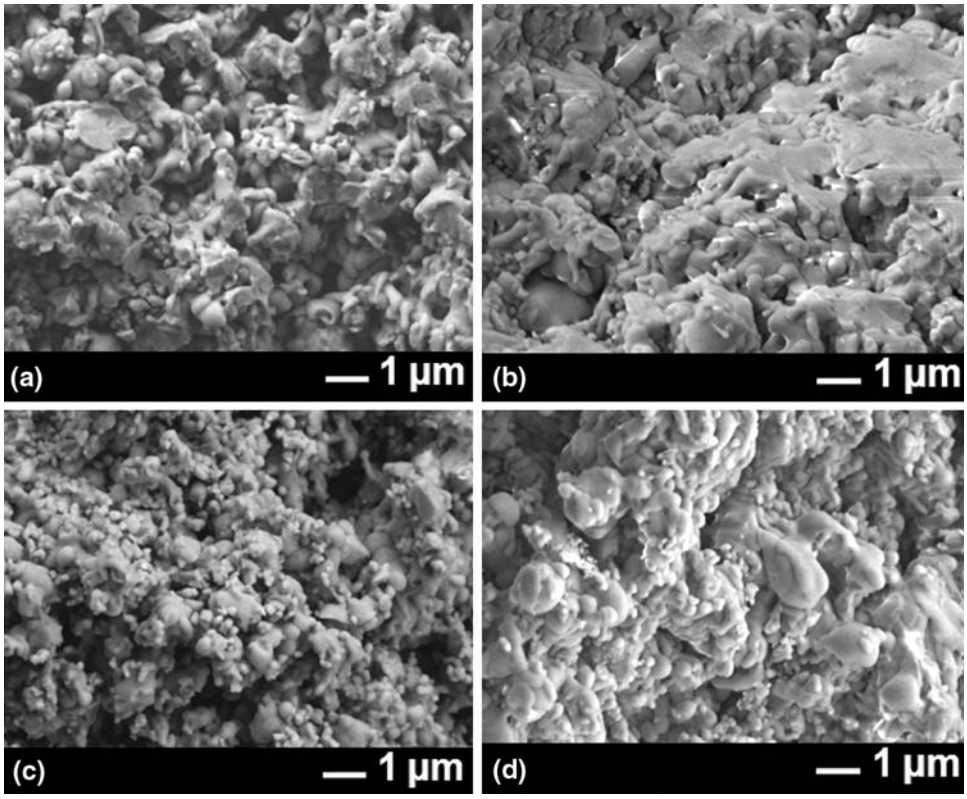

Fig. 6 FESEM views of fractures of different alumina coatings manufactured with different parameters: (a) 172A, (b) 30A, (c) 30B, and (d) 30C

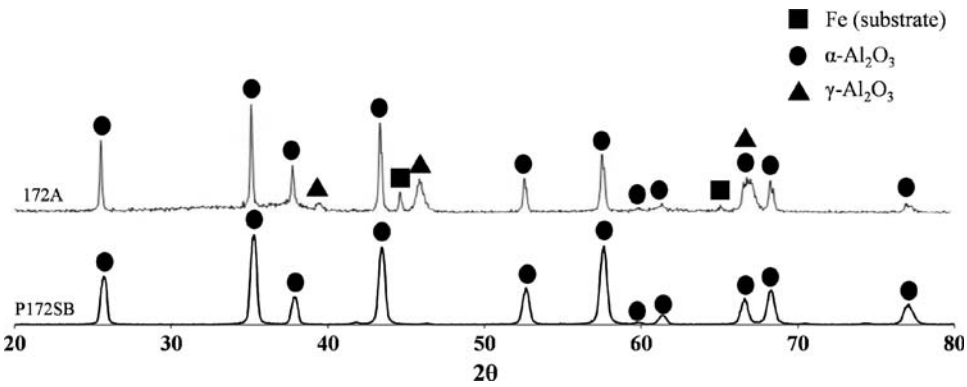

Fig. 7 X-ray diffraction patterns of P172SB powder and corresponding coating (172A)

plasma flow (Ref 12). This phenomenon is indirectly confirmed by the wear rate results (Table 3). Indeed, embedded granular and spherical particles weaken the coatings due to meager bridges between particles. When the contact load is applied during sliding test, coating is more easily worn due to particle exfoliation. Moreover, it appears when comparing friction curves, the one corresponding to the 30A operating parameter set (Ar-He plasma gas mixture) is less fluctuating than the one corresponding to the 30C operating parameter set (Ar-H_2 plasma gas mixture). This is the result of a lower defect density in wear track and a better coating cohesion. Then, with an Ar-H_2 plasma gas mixture, decreasing enthalpy (30B) leads to a coating which exhibits a slightly higher friction coefficient but mostly a wear rate 4 times higher because of the presence of a higher fraction of poorly or even untreated particles, decreasing the cohesion between grains or lamellae. Therefore, lower plasma mass enthalpy and higher amplitude in arc root fluctuations lead to more stacking defects in coatings which decreased their cohesive strength.

In order to establish a comparison with a previously published study (Ref 13), sliding tests have been undertaken considering coatings manufactured on a smooth

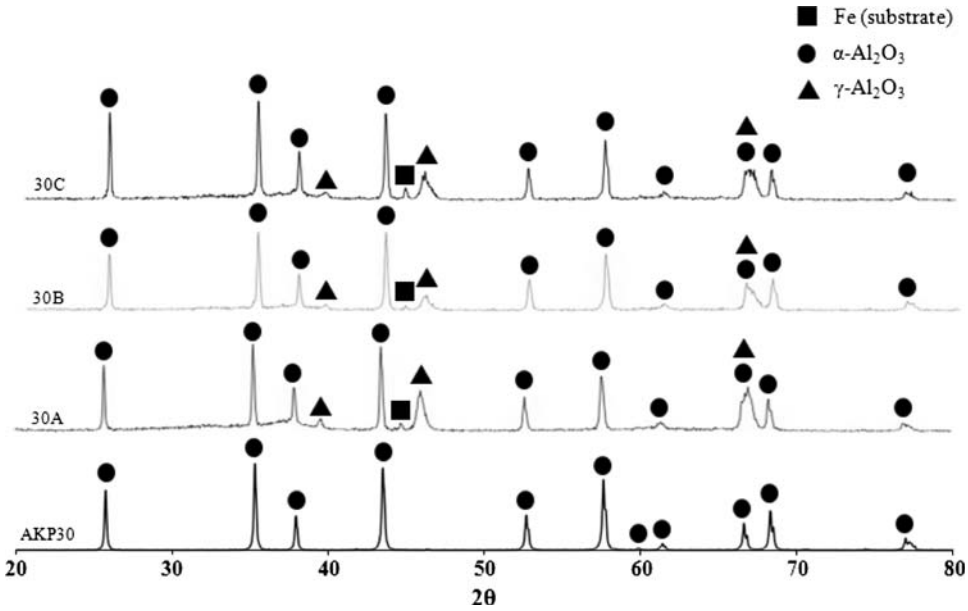

Fig. 8 X-ray diffraction patterns of AKP30 powder and corresponding coatings (30A, 30B, and 30C)

Table 4 Surface parameters of Ball-on-disc samples after polishing protocols (see Table 1 for designation)

Designation	172A	30A	30B	30C	30As	ZrA	SiA
Ra, μm	2.38 ± 0.21	2.36 ± 0.19	3.17 ± 0.26	4.87 ± 0.54	2.50 ± 0.24	2.61 ± 0.52	2.31 ± 0.16
Rz, μm	14.83 ± 1.14	14.86 ± 1.12	17.45 ± 1.37	26.25 ± 2.93	13.48 ± 1.19	14.73 ± 2.39	13.71 ± 1.51
RSk	−1.52 ± 0.14	−1.74 ± 0.30	−1.03 ± 0.09	−0.25 ± 0.17	−0.22 ± 0.09	−1.29 ± 0.34	−1.33 ± 0.27
RKu	6.14 ± 1.05	7.02 ± 1.68	3.94 ± 0.44	2.83 ± 0.31	2.58 ± 0.11	5.12 ± 2.00	5.03 ± 1.73
RSm, μm	74.53 ± 4.28	83.58 ± 3.25	85.94 ± 5.99	98.65 ± 8.53	63.29 ± 5.40	88.66 ± 9.29	77.54 ± 4.89
RHTp, μm	4.51 ± 0.35	4.34 ± 0.45	6.56 ± 0.57	10.56 ± 1.03	5.58 ± 0.54	5.25 ± 1.08	4.53 ± 0.22

Average values and associated standard deviations from eight values resulting from ten randomly located measurements with an adjustment of 20%

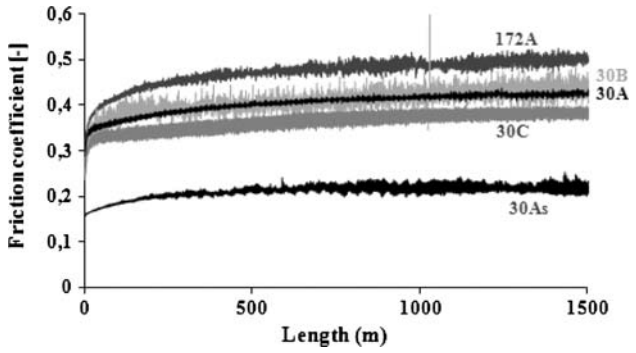

Fig. 9 Friction coefficient vs. sliding distance for SPS Al_2O_3 sub-micrometric-sized coatings manufactured with different operating parameters and feedstock powders (test parameters depicted in Sect 2.3)

(i.e., polished) substrate. Polishing of the substrate permits to adapt its roughness to the particle average size. Indeed, mechanical anchoring is the assumed adhesion mechanism of SPS coatings. Mechanical anchoring requires the average substrate roughness to be of the same order as the average thicknesses of lamellae. In conventional atmospheric plasma spraying (APS), the average particle diameter of ceramic feedstock is in the order of 30 μm, and the average thickness of the lamellae, assuming a flattening ratio of 3 to 4, is about 1-2 μm. Grit-blasting substrates permits to generate an average roughness of this order. In SPS, average particle diameter is much lower, down to 50 nm in the present case. Assuming flattening ratios of 1-2, average thicknesses of lamella is about 25-50 nm. Polishing of the substrates permits to generate such an average roughness. A limitation in polishing substrates resides in the maximal ''dense'' coating thickness that can be manufactured: this limitation seems to be in the order of 30 μm with the considered operating conditions. At higher thickness, stacking defects develop through the coating thickness as depicted in Fig. 10 due to a so-called shadow effect induced by the substrate surface anfractuosities. It was demonstrated in Ref 13 that decreasing the structural scale of alumina coatings was lowering its friction coefficient together with its wear rate. Friction coefficient against sintered α-Al_2O_3 of APS coating manufactured with α-Al_2O_3 of $d_{50} = 36$ μm was 0.8-0.9 whereas the one of a SPS coating manufactured

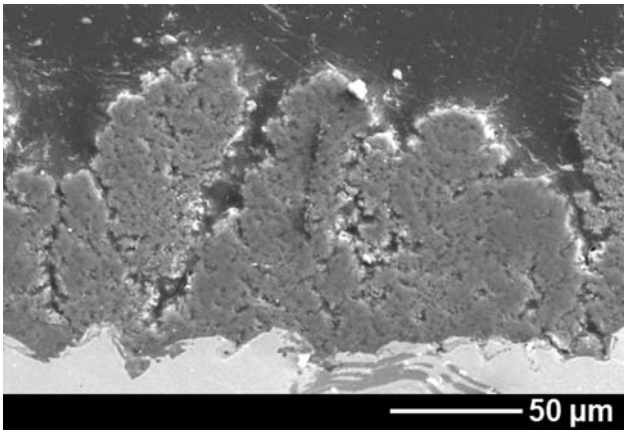

Fig. 10 Stacking defects developing through a SPS coating thickness manufactured onto a substrate exhibiting a surface roughness far higher than the feedstock average size

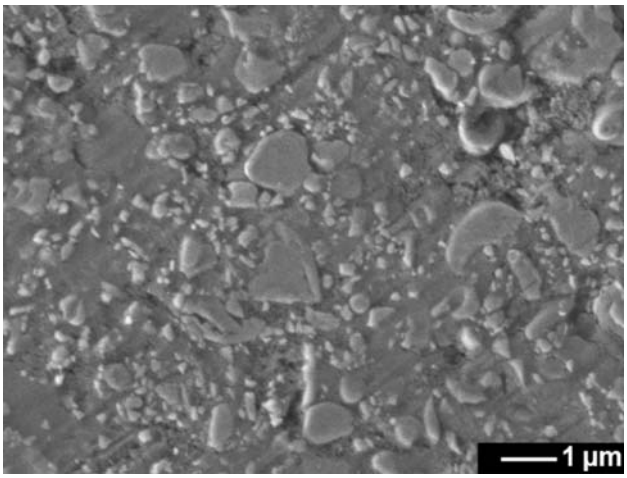

Fig. 11 Wear tracks (FESEM) of Al_2O_3 sub-micrometer-sized coatings made with P152SB powder (Ref 13) (1500 m sliding distance, α-Al_2O_3 ball of 6 mm in diameter, 2 N load, relative speed of 0.1 m s^{-1})

with α-Al_2O_3 of $d_{50} = 1.3$ µm was 0.4-0.5. Even a further reduction of the particle average size down to $d_{50} = 0.3$ µm (AKP30 referenced 30As in Fig. 9) permits to decrease the friction coefficient to 0.2. The smaller the coating structural scale, the lower the friction coefficient. Also, the friction coefficient of the coating manufactured with these latter conditions (30As) is lower than the one of the coating manufactured with identical spray parameters on a grit-blasted substrate (30A). This evidences once again that coating cohesion is decreased when manufactured onto a rough surface due to the development of stacking defects through the coating thickness.

Wear mechanisms of alumina SPS coatings were also investigated. In the case of the P152SB powder ($d_{50} = 1.3$ µm), wear track is depicted in Fig. 11. Two characteristic features are observed: the first one appears like a ''matrix'' whereas the second one appears like particles embedded in the matrix. An assumption could be that the so-called matrix is predominantly made of γ-Al_2O_3 and embedded particles made of α-Al_2O_3 particles. Nevertheless, x-ray analysis points out (152 x-ray pattern is similar to 172 one) that γ phase represents only about 20% of the constitutive material, and the so-called matrix represents a higher ratio, estimated to be about 55%. Studies are underway to further understand this very typical coating architecture. The very low wear rate of such an SPS coating (about 30 times lower than a conventional APS one in same test conditions as new measurements using a device with a higher resolution compared to measurements presented in Ref 13 have shown) can be very likely explained by the wear of the embedded particles, and not by their exfoliation since no delaminations nor cracks nor grooves have been observed, in particular, at the interfaces between the so-called matrix and embedded particles, emphasizing the high cohesion/high toughness of such coatings. Hence, only plastic deformation occurs on these mono crystalline particles forming the coating, reducing drastically its wear rate (once again, the coating is uniformly worn without exfoliation of particles and lamellae).

In this section, some observations already made have been confirmed. Owing to the decrease in the feedstock size, the friction coefficient of the resulting coating is reduced. With a lower grain size, the number of interfaces at grain boundaries increases leading to a lower wear rate. The importance of the choice of plasma forming gases on the coating performances has also been evidenced. Arc root fluctuations lead to poorer thermal treatment of particles, decrease in turn coating cohesion, and increase in its friction coefficient and wear rate.

3.2 Composite Coatings

Several composite coatings have also been manufactured and their tribological behaviors assessed: Al_2O_3-ZrO_2 and Al_2O_3-SiC coating behaviors will be discussed hereafter.

3.2.1 Coating Structures. Figure 12 presents the structure of Al_2O_3-ZrO_2 and Al_2O_3-SiC coatings made with operating condition A. All of them seem rather dense while polishing artifacts. Also, zirconia reinforcement particles (in white in Fig. 12a) are well dispersed inside the alumina matrix. Figure 13 presents phase compositions of manufactured composite coatings. ZrA coating contains tetragonal ZrO_2 and the two phases of Al_2O_3, α and γ. SiA coating is made of α and γ-Al_2O_3, SiC with well-defined peaks and a very low amount of SiO_2. This corresponds very likely to the oxidation of the periphery of SiC particles either during their flight or after being embedded in the coating structure (between two successive passes of the plasma torch in front of the same location). Such a surprisingly low oxidation rate could result from the combination of two mechanisms: (i) a reduced surrounding atmosphere entrapment due to the short spray distance (30 mm) and (ii) the rarefaction effect due to the small particle size. Pfender (Ref 17) was among the very first researchers to measure the plasma flow oxygen

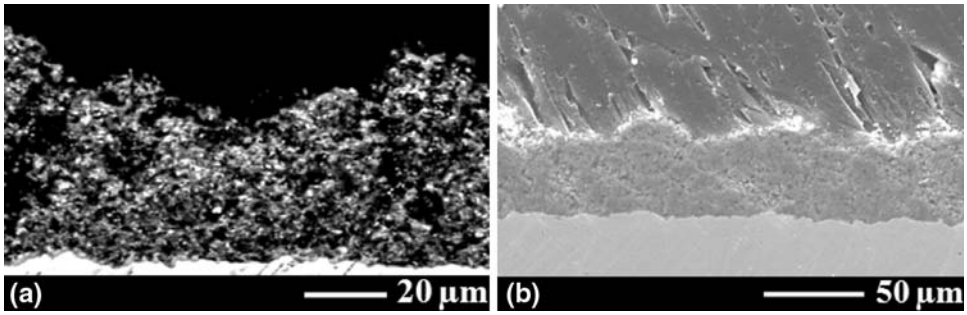

Fig. 12 BSE-SEM view of (a) Al_2O_3-ZrO_2 (ZrA) and SE-SEM view of (b) Al_2O_3-SiC (SiA) composite coating cross sections

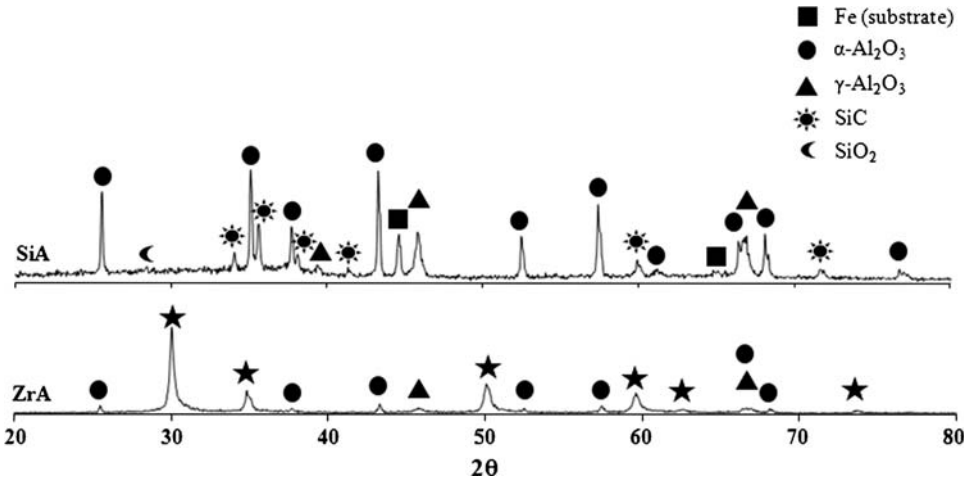

Fig. 13 X-ray diffraction patterns of composite coatings Al_2O_3-ZrO_2 (ZrA) and Al_2O_3-SiC (SiA)

concentration profiles resulting from surrounding atmosphere entrapment versus distance from the torch nozzle exit: at short distances (typically below 40 mm), the surrounding atmosphere entrapment within the plasma flow remains very limited due to the high viscosity/high momentum density of the plasma potential core. Chen and Pfender (Ref 18) demonstrated that at atmospheric pressure, non-continuity effects, known as Knudsen effect, become emphasized for particles smaller than 10 µm immersed in a thermal plasma flow. When the molecular mean free path ceases to be negligible in front of the particle size, the Nusselt number, depicting the dimensionless thermal gradient at the particle wall under forced convective heat transfer regime, is drastically decreased (the heat flux is not anymore proportional to the exchange surface), corresponding to a decrease in the heat flux transferred to the particles. Those two mechanisms can take place in the considered conditions (their relative contribution are unknown) and can lead to a decrease in SiC particle temperature together with a reduced exposure to oxygen.

3.2.2 Friction Coefficient and Wear Rate. The friction coefficient versus sliding distance of composite coatings is displayed in Fig. 14. While comparing with the reference curve (i.e., 30A), the ZrA composite coating exhibits a higher friction coefficient (40% higher than pure Al_2O_3 coating sprayed with identical operating parameters). This is intrinsic to the presence of zirconia particles within the coating. *A. contrario*, the wear rate is decreased by about 15%. This could be attributed to the better resistance to

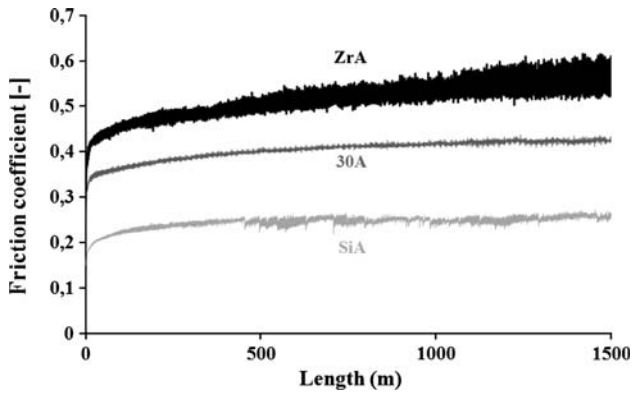

Fig. 14 Friction coefficient vs. sliding distance for composite Al_2O_3 sub-micrometric-sized coatings manufactured with different operating parameters and feedstock powders (test parameters depicted in Sect 2.3)

crack propagation provided by zirconia, as demonstrated by Wang et al. (Ref 19). However, for SiA coating, the reverse behavior is observed with a lower friction coefficient and a wear rate that is slightly higher. Silicon carbide has a better sliding behavior than alumina, and, therefore, very likely the friction coefficient is improved. However, wear rate is higher, and this is likely due to the significant difference in average sizes of Al_2O_3 and SiC powders. The wear rate is very different when a particle of 3 μm is exfoliated rather than the one of 400 nm. Studies are underway with SiC powder of average size of about 400 nm.

4. Conclusions

This study aimed at manufacturing, by suspension plasma spraying, ceramic and composite coatings having superior tribological behaviors. SPS seems suitable to preserve feedstock composition, even with material showing high vapor pressure such as SiC.

Friction study corroborated that by decreasing the feedstock average size, the sliding behavior is improved (friction coefficient is decreased). Indeed, feedstock size distribution and plasma forming gases play both relevant roles in coating microstructure and mechanical behavior. Also, the addition of SiC in alumina matrix permits to decrease the coating friction coefficient. Al_2O_3/ZrO_2 exhibit a better wear resistance than pure Al_2O_3.

Acknowledgments

This study was conducted within the framework of the French FCE-NANOSURF consortium (Mecachrome, Frechin, CRT Plasma Laser, Cilas, CEA, CITRA, and SPCTS) that is granted by the French Ministry and Industry and local governments of *Région Centre* and *Limousin*, the financial supports from whom are gratefully acknowledged by the authors.

References

1. S.C. Tjong and H. Chen, Nanocrystalline Materials and Coatings, *Mater. Sci. Eng. R*, 2004, **45**(1-2), p 1-88
2. R. Gadow, F. Kern, and A. Killinger, Manufacturing Technologies for Nanocomposite Ceramic Structural Materials and Coatings, *Mater. Sci. Eng. B*, 2008, **148**(1-3), p 58-64
3. I. Garcia, J. Fransaer, and J.P. Celis, Electrodeposition and Sliding Wear Resistance of Nickel Composite Coatings Containing Micron and Submicron SiC Particles, *Surf. Coat. Technol.*, 2001, **148**(2-3), p 171-178
4. T. Chraska, K. Neufuss, J. Dubsky, P. Ctibor, and P. Rohan, Fabrication of Bulk Nanocrystalline Alumina Zirconia Materials, *Ceram. Int.*, 2008, **34**(5), p 1229-1236
5. R.S. Lima, A. Kucuk, and C.C. Berndt, Evaluation of Microhardness of Thermally Sprayed Nanostructured Zirconia Coatings, *Surf. Coat. Technol.*, 2001, **135**(2-3), p 166-172
6. X. Zhao, Y. An, J. Chen, H. Zhou, and B. Yin, Properties of Al_2O_3-40wt.%ZrO_2 Composite Coatings from Ultra-fine Feedstocks by Atmospheric Plasma Spraying, *Wear*, 2008, **265**(11-12), p 1642-1648
7. E.H. Jordan, M. Gell, Y.H. Sohn, D. Goberman, L. Shaw, S. Jiang, M. Wang, T.D. Xiao, Y. Wang, and P. Strutt, Fabrication and Evaluation of Plasma Sprayed Nanostructured Alumina/Titania Coatings with Superior Properties, *Surf. Coat. Technol.*, 2003, **167**(1), p 68-76
8. Y. Zhou, H. Zhang, and B. Qian, Friction and Wear Properties of the Co-Deposited Ni-SiC Nanocomposite Coatings, *Appl. Surf. Sci.*, 2007, **253**(20), p 8335-8339
9. L.L. Shaw, D. Goberman, R. Ren, M. Gell, S. Jiang, Y. Wang, T.D. Xiao, and P.R. Strutt, The Dependency of Microstructure and Properties of Nanostructured Coatings on Plasma Sprayed Conditions, *Surf. Coat. Technol.*, 2001, **130**(1), p 1-8
10. L. Pawlowski, Finely Grained Nanometric and Submicronic Coatings by Thermal Spraying, *Surf. Coat. Technol.*, 2008, **202**(18), p 4318-4328
11. P. Fauchais, R. Etchard-Salas, V. Rat, J.-F. Coudert, N. Caron, and K. Wittmann-Ténèze, Parameters Controlling Liquid Plasma Spraying: Solutions, Sols, or Suspensions, *J. Therm. Spray Technol.*, 2008, **17**(1), p 31-59
12. R. Etchart-Salas, ''d.c. Plasma Spraying of Suspensions of Submicronic Particles. Experimental and Analytic Approaches of Phenomena Implied in the Reproducibility and Quality of Coatings'', Ph.D. thesis, University of Limoges, 2007 (in French)
13. G. Darut, H. Ageorges, A. Denoirjean, G. Montavon, and P. Fauchais, Effect of the Structural Scale of Plasma Sprayed Alumina Coatings on Their Friction Coefficients, *J. Therm. Spray Technol.*, 2008, **17**(5-6), p 788-795
14. L.C. Erickson, T. Troczynski, H.M. Hawthorne, H. Tai, and D. Ross, Alumina Coatings by Plasma Spraying of Monosize Saphire Particles, *J. Therm. Spray Technol.*, 1999, **8**(3), p 421-426
15. C. Delbos, ''Contribution to the Understanding of Ceramic (Y-PSZ, Perovskite, etc.) or Metallic (Ni, etc.) Particles Injection by a Liquid Carrier in a Plasma Jet to Manufacture Finely-Structured Coatings for SOFC'', Ph.D. thesis, University of Limoges, France, 2004 (in French)
16. Z. Duan and J. Heberlein, Arc Instabilities in a Plasma Spray Torch, *J. Therm. Spray Technol.*, 2002, **11**(1), p 44-51
17. E. Pfender, Fundamental Studies Associated with the Plasma Spray Process, *Surf. Coat. Technol.*, 1988, **34**, p 1-14
18. X. Chen and E. Pfender, Effect of the Knudsen Number on Heat Transfer to a Particle Immersed into a Thermal Plasma, *Plasma. Chem. Plasma Process.*, 1983, **3**(1), p 97-114
19. Y.S. Wang, C. He, B.J. Hockey, P.I. Lacey, and S.M. Hsu, Wear Transitions in Monolithic Alumina and Zirconia-Alumina Composites, *Wear*, 1995, **181-183**(1), p 156-164